Journal of
Materials Chemistry A

Accepted Manuscript

This is an *Accepted Manuscript*, which has been through the RSC Publishing peer review process and has been accepted for publication.

Accepted Manuscripts are published online shortly after acceptance, which is prior to technical editing, formatting and proof reading. This free service from RSC Publishing allows authors to make their results available to the community, in citable form, before publication of the edited article. This *Accepted Manuscript* will be replaced by the edited and formatted *Advance Article* as soon as this is available.

To cite this manuscript please use its permanent Digital Object Identifier (DOI®), which is identical for all formats of publication.

More information about *Accepted Manuscripts* can be found in the **Information for Authors**.

Please note that technical editing may introduce minor changes to the text and/or graphics contained in the manuscript submitted by the author(s) which may alter content, and that the standard **Terms & Conditions** and the **ethical guidelines** that apply to the journal are still applicable. In no event shall the RSC be held responsible for any errors or omissions in these *Accepted Manuscript* manuscripts or any consequences arising from the use of any information contained in them.

Flexible Symmetrical Planar Supercapacitors Based on Multi-Layered MnO_2/Ni/Graphite/Paper Electrodes with High-Efficient Electrochemical Energy Storage

Jin-Xian Feng, Qi Li, Xue-Feng Lu, Ye-Xiang Tong, and Gao-Ren Li*

MOE Laboratory of Bioinorganic and Synthetic Chemistry, KLGHEI of Environment and Energy Chemistry, School of Chemistry and Chemical Engineering, Sun Yat-sen University, Guangzhou 510275, China

E-mail: ligaoren@mail.sysu.edu.cn

High-performance planar supercapacitors have attracted increasing attention because of their thin, light and flexible ability. Here we developed novel flexible symmetrical planar supercapacitors (FSPSCs) by using the multi-layered MnO_2/Ni/graphite/paper electrodes that were fabricated by sequentially coating graphite layer, Ni layer, and MnO_2 layer on the ordinary cellulose paper. The MnO_2/Ni/graphite/paper electrodes show large specific capacitance (C_{sp}) of 175 mF/cm^2 at a scan rate of 5 mV/s and excellent cycle stability (less 4% loss of the maximum C_{sp} after 6000 cycles). The assembled FSPSCs based on the multi-layered MnO_2/Ni/graphite/paper electrodes exhibit large volumetric C_{sp} (1020 mF/cm^3 at 5 mV/s) and superior long-term cycle stability (less 4% loss of the maximum C_{sp} after 6000 cycles). The FSPSCs based on the multi-layered MnO_2/Ni/graphite/paper electrodes would open up new opportunities in developing novel supercapacitor devices because of the low-cost, high performance, and facile large-scale fabrication procedures.

Keywords: MnO_2/Ni/graphite; sandwich-like structure; paper electrode; flexible; planar supercapacitor

Introduction

Increasing power and energy demands for next-generation portable and flexible electronics such as roll-up displays, photovoltaic cells, and wearable devices has inspired intensive efforts to explore the flexible, light-weight, and environmentally friendly energy storage devices.[1-4] The flexible solid-state supercapacitors (SCs) represent a new class of energy storage devices that can provide high specific gravimetric/volumetric energy and power densities for flexible electronics.[5-8] Recently, great efforts have been dedicated to achieve thin, light-weight, and flexible supercapacitors.[9-12]

Planar SCs, as a new emerging branch of electrochemical capacitors, can enable the entire device to be thin and flexible.[13-15] Paper electronics have been a dream of the next-generation electronics. The electrolyte ions are transported two-dimensionally in such device, and accordingly shorten ion travel distance. In addition, the planar SCs significantly decrease the thickness in vertical direction and rather expand along 2D horizontal planes, making compact device design possible.[16-19] However, up to now, the exploitation of high-performance planar SCs is not sufficient.

Recently, the paper electrodes have attracted much interest for the development of planar SCs.[14] The cellulose paper, is a kind of low cost and abundant material, which has excellent flexible ability. The intrinsic rough and porous surfaces of paper are ideal for energy devices in which large surface roughness is beneficial for the manipulation of electrons and ions. However, the cellulose paper is a insulator. To enhance the conductivity of paper, the carbon nanotubes are usually coated on the surface of paper through a solution-based process. This process usually involves environmentally unfriendly chemicals and elaborate procedures, and the cost of carbon nanotubes is still prohibitive.[20] In addition, the graphene is employed to cover paper. But the graphene is also prohibitive and is usually fabricated by the harsh oxidation-reduction process at high temperature. Recently, Cui *et al* developed a simple and economical drawing method to draw a layer of graphite on a piece of ordinary cellulose paper to fabricate paper electrode for planar SCs.[21] However, to the best of our knowledge, up to now, the performance such as specific capacitance (C_{sp}) and power/energy densities of paper electrode is relative low, and there is no effective method to improve the performance of planar SCs.

Based on the above considerations, in this study we develop a novel multilayered MnO_2/Ni/graphite/paper electrodes with high performance for planar SCs. The aims of designing such multilayered MnO_2/Ni/graphite/paper electrodes are listed as following: (*i*) The paper is flexible, thin and light; (*ii*) The bottom graphite layer can be easily drawn with regular pencil on cellulose paper. Accordingly, the thin graphite layer can obviously enhance the conductivity of paper; (*iii*) The homogeneous Ni layer can be easily electrodeposited on the graphite/ paper, and it will provide electron "superhighways" for charge storage and delivery because of its excellent electrical conductivity, which will overcome the key weakness (the limited electric conductivity) of MnO_2 and further enhance the conductivity of electrode; (*iv*) MnO_2 has been recognized as the most promising electrode material for SCs because of its low-cost, good electrochemical reactivity and environmental compatibility.[22-26] (*v*) The MnO_2 nano-sheet can provide large surface area which will greatly enhance the electroactive surface area. Recent work shows that the SCs based on MnO_2 films grown on the conductive substrates exhibit high performance.[27-30] Electrochemical measurements show that the designed MnO_2/Ni/graphite/paper multi-layered electrodes exhibit high performance. Here the flexible symmetrical planar supercapacitors (FSPSCs) are assembled by using the multi-layered MnO_2/Ni/graphite/paper electrodes, and they exhibit large volumetric C_{sp} (1000 mF/cm^3 at 5 mV/s) and superior long-term cycle stability (less 4% loss of the maximum specific capacitance after 3000 cycles). These findings indicate that the multi-layered MnO_2/Ni/graphite/paper electrode is a promising material for FSPSCs.

Results and Discussion

The schematic illustration of the procedure used to fabricate the multi-layered MnO_2/Ni/graphite/paper electrodes is shown in Scheme 1a. The homogeneous graphite layer is firstly drawn on a cellulose paper to form the graphite/paper. The loading mass of graphite on paper is about 0.51mg·cm^{-2}. Optical image in Figure 1b shows that the thin graphite layer is uniform on paper. The electrical resistance of the graphite/paper sheets (2 cm × 2 cm) is about 2000 Ω, which is much lower than that of the cellulose paper with the same size (>20 MΩ). The resistance is almost equal in every corner of the paper. So the

thin graphite layer greatly reduces the resistance of the cellulose paper. After this, the homogeneous thin Ni layer is electrodeposited on the graphite/ paper to form the Ni/graphite/paper. Optical image in Figure 1c shows that the Ni layer is also uniform. After coating Ni layer, the resistance of the Ni/graphite/paper is further greatly reduced to 1.6 Ω. So the paper-like substrate with high conductivity is fabricated. Finally, the homogeneous MnO_2 layer is electrodeposited on the Ni/graphite/ paper and accordingly the multi-layered MnO_2/Ni/graphite/paper electrode is fabricated. The optical image in Figure 1d shows that the MnO_2 layer is uniformly coated on the Ni/graphite/paper. The details of fabrication are described in the experimental section in supporting information.

Figure 1(e-h) shows SEM images of surface morphology of paper, graphite/paper, Ni/graphite/paper and MnO_2/Ni/graphite/paper, respectively. We clearly see the surface of cellulose papers is rough and porous. The surfaces of graphite layers and Ni layers are uniform as shown in Figure 1(f-g), respectively. The MnO_2 layers grown on the Ni/graphite/paper have sponge-like porous morphology with pores of 300~500 nm, which would relax the transport of electroactive species, enable fast electrochemical reactions and provide short diffusion paths for electroactive species. The porous structures would also obviously enhance the utilization rate of MnO_2. The cross sections of graphite/paper, Ni/graphite/paper, and MnO_2/Ni interfaces in the MnO_2/Ni/graphite/paper are shown in Figure 1(i-k), which shows the thicknesses of graphite layer, Ni layer, and MnO_2 layer are about 15, 2, and 1 μm, respectively. In addition, the MnO_2 layer grown on Ni layer is rather firmly. To further characterize the morphology of the MnO_2 layer, TEM, HRTEM and SAED were measured and the results are shown in Figure S1. These result shows MnO_2 nanosheets have polycrystalline structures.

Figure 2a shows Raman spectrum of graphite layer on paper, and two peaks appear at 1358 and 1583 cm^{-1}. These two peaks are in consistent with the graphite. XPS spectra of the MnO_2/Ni/graphite/paper electrode in Ni 2*p* and Mn 2*p* regions were measured. Figure 2b shows the Ni $2p_{3/2}$ peak is centered at 856.5 eV with a shakeup satellite at about 6.5 eV higher bonding energy and the Ni $2p_{1/2}$ peak is centered at 874.1 eV with a shakeup satellite at about 6.8 eV higher bonding energy. These Ni 2p binding energies are consistent with the typical values of metal Ni.[31] The Mn 2p spectrum in Figure 2c

shows the Mn $2p_{3/2}$ and Mn $2p_{1/2}$ binding energies are centered at 642.2 and 654.3 eV, respectively, which are consistent with the typical values of Mn(IV).[32] The result of XPS spectrum in Figure 2d confirms that the existence of O^{2-}, which coming from Mn-O-Mn and the adsorbed H_2O.[32] So the above results prove the existence of MnO_2. XRD patterns of the Ni/graphite/paper and MnO_2/Ni/graphite/paper are shown in Figure 2e. For Ni/graphite/paper, the Ni phase is clearly seen, indicating that the pure Ni layer was fabricated. For the MnO_2/Ni/graphite paper electrodes, the peaks of MnO_2 are clearly seen besides Ni peaks as shown in Figure 2e, indicating the polycrystal MnO_2 layers were fabricated. The specific surface area calculated by the Brunauer-Emmett-Teller (BET) method is *ca*. 77.85 m^2/g (Figure S2), and the pore size is average 7 nm. The above results show a large surface area and small pores in electrodes.

Here the conductibility of the multilayered MnO_2/Ni/graphite/paper electrodes is studied by electrochemical impedance spectroscopy (EIS). Nyquist plots of the MnO_2/Ni/graphite/paper electrode and MnO_2/graphite/paper electrode (without Ni layer) between 1 and 10 kHz are shown in Figure 2f. For the MnO_2/Ni/graphite/paper electrode, a much lower equivalent series resistance (ESR) and a more vertical line in the low-frequency region are seen, indicating that the MnO_2/Ni/graphite/paper electrodes have a much higher conductivity than the MnO_2/graphite/paper electrodes. This shows that the Ni layers can obviously reduce the internal resistance of electrode, thus improving the transport and collection of electrons in electrode. The high conductibility in electrode will favor rate capability for high power performance and fast charge-discharge. The utilization rate of electrode material will be largely enhanced by the high conductibility of electrode because of slight polarization.

To evaluate the electrochemical performance of multilayered MnO_2/Ni/graphite/paper electrodes, the electrochemical measurements were conducted in a three-electrode system with a Pt wire as counter electrode and a saturated calomel electrode (SCE) as reference electrode. The loading amount of MnO_2 is average 0.25 mg/cm^2. Cyclic voltammograms (CVs) of the MnO_2/Ni/graphite/paper electrodes in a three-electrode system at different scan rates are shown in Figure 3a, which shows nearly rectangular shape for all CV curves, indicating the symmetric current-potential characteristics and good

supercapacitive properties. The C_{sp} of the MnO_2/Ni/graphite/paper electrodes at 5 mV/s is calculated 170 mF/cm^2 (680 F/g), which is much higher than those MnO_2 nanobar deposit on carbon clothes(625 F/g),[33] hierarchical tubular MnO_2 structures (315 F/g),[34] MnO_2 nanotube/nanofibre (461 F/g),[35] and MnO_2-carbon nanotube sponges (240 F/g).[36] The dependence of C_{sp} on scan rate is shown in Figure 3b, which shows a decay of 35% in the C_{sp} of the MnO_2/Ni/graphite/ paper electrodes with scan rate increasing from 5 to 100 mV/s. Even at a scan rate as high as 100 mV/s, the MnO_2/Ni/graphite/paper electrodes still achieve a C_{sp} as large as 110 mF/cm^2 (440 F/g). However, for MnO_2 tube/nanofibre and MnO_2-carbon nanotube sponges, they only showed 241 F/g and 120 F/g, respectively, at 100 mV/s, and their C_{sp} values all show a decay of ~40% with scan rate increasing from 5 to 100 mV/s.[34-35] So the MnO_2/Ni/graphite paper electrodes show much larger C_{sp} at all scan rates and much better rate capability than MnO_2 nanobar, hierarchical tubular MnO_2 structures, MnO_2 tube/nanofibre, and MnO_2-carbon nanotube sponges.

In order to illustrate the effect of MnO_2 on the performance of the multi-layered MnO_2/Ni/graphite/ paper electrodes, Figure 3c compares the CVs of electrodes with different deposition time of MnO_2 from 10 to 35 min. It can be seen that all these curves exhibit nearly rectangular shape, indicating the ideal supercapacitive behavior. Among of these different electrodes, the MnO_2/Ni/graphite/paper electrodes with MnO_2 deposition time of 30 min exhibit the highest C_{sp} of 107 mF/cm^2 (428 F/g) at 100 mV/s.

Figure 3d shows the galvanostatic charge-discharge curves of the MnO_2/Ni/graphite/paper electrodes in three-electrode system at various current densities. The discharge curves all are well symmetrical with their corresponding charge counterparts, and a good linear relation of discharge-charge voltage versus time is identified. This confirms the ideal capacitive characteristic and rapid charge-discharge property of the multi-layered MnO_2/Ni/graphite/paper electrodes. With charging-discharging rate increasing from 0.5 to 4.0 mA/cm^2, the C_{sp} decreases from 125 to 100 mF/cm^2 (500 to 400 F/g) and the loss is less than 30% while MnO_2 tube/nanofiber, and MnO_2-carbon nanotube sponges showed more than 45% C_{sp} loss.[33-36] So this result demonstrates that the MnO_2/Ni/graphite/paper electrodes have a

much better rate capability than the other MnO_2 electrodes. The C_{sp} of MnO_2/Ni/graphite/paper electrodes is substantially higher than the MnO_2 nanobar, hierarchical tubular MnO_2 structures, MnO_2 tube/nanofiber, and MnO_2-carbon nanotube sponges.[33-36] The enhanced electrochemical performance of the MnO_2/Ni/graphite/paper electrodes can be attributed to the special MnO_2/Ni/graphite sandwich-structures and sponge-like structure of MnO_2: (*i*) The conductive networks in electrode are well-built since the MnO_2 layers are attached tightly on Ni layers that will provide electron "superhighways" for charge storage and delivery because of the high electrical conductivity; (*ii*) The sponge-like structure of MnO_2 will create efficient diffusion paths for electrolyte ions, which will significantly enhance the intercalation of ions and utilization rate of electrode material.

To realize the application for energy storage device, the flexible symmetrical planar supercapacitor (FSPSC) based on the MnO_2/Ni/graphite/paper electrodes were assembled as shown in Scheme 1b. The carboxymethyl cellulose sodium (CMC)/Na_2SO_4 gel was used as solid-state electrolytes. The average thickness of well-assembled FSPSC is 1.0 mm, the average weight of electrode is 7.5 mg/cm^2, and the whole FSPSC is average 16 mg. All the results are based on the entire device including the electrolyte and electrodes. The assembled solid state FSPSC has excellent flexibility and well mechanical properties and can undergo blending to different angles and twisting as shown in Figure 4(a-c). CVs of the solid-state FSPSC were measured in a two-electrode system at various scan rates and they are shown in Figure 4d. All of these CVs exhibit rectangular-like shapes even at a high scan rate of 100 mV/s, and this reveals the good capacitive behavior of FSPSC. This solid-state device shows a large volumetric C_{sp} of 1020 mF/cm^3 at 5 mV/s (based on the entire device including the electrolyte and electrodes) and has a good rate capability. More importantly, the electrochemical performance of the FSPSC almost has no change under various distortion situations and remain almost the same while it change from normal state to 180^o and then recover to normal state as shown in Figure 4e, further confirming that the FSPSC have remarkable mechanical flexibility.

Figure 4f shows the galvanostatic charge-discharge curves of the FSPSC measured in two-electrode system at different current densities. The discharge curves of the FSPSC device are relatively

symmetrical with its corresponding charge counterparts, confirming good capacitive behavior and fast charge-discharge behavior of the FSPSC. The calculated volumetric C_{sp} (based on the entire device including both the electrolyte and electrodes) are 532, 482, 432 and 372 mF/cm^3 (33.2, 30.0, 27.0 and 23.0 F/g) at the current densities of 0.5, 1.0, 2.0 and 4.0 mA/cm^2 and 704, 742, 890, 924 and 1020 mF/cm^3 (44.0, 64.2, 55.6 and 63.6 F/g) at the scan rates of 5, 10, 20, 50 and 100 mA/cm^2, respectively. The maximum energy density and power density of the FSPSC device are determined to be 106 mWh/cm^3 (56.2 Wh/kg) and 48 mW/cm^3 (60.0 kW/kg) as shown in Figure 4g. The cell-voltage is also a critical para-meter in determining the energy and power performance of supercapacitors. Here we compare the CV curves which are obtained at the scan rate of 100 mV/s from 0.8 V to 1.5 V as shown in Figure S6a. From this graph, we can clearly see that the FSPSC remain stable at the potential window of 0.8~1.2 V. However, when the potential window is higher than 1.5 V, the CV curve become sharp and its shape is apart from rectangular, and the capacitance retention only remains about 84 % after 1500 cycles and 74 % after 3000 cycles (Figure S6b). When the potential is 1.2 V, the FSPSCs show high cycle stability and the capacitance retention remains about 97 % after 3000 cycles. The volumetric capacitance at 0.8, 1.0, 1.2 and 1.5 V is 456.6, 784.0, 748.4, 885.4 mF/cm^3, respectively, the energy density is 24.3, 48.2, 69.4 and 138.0 mWh/cm^3, respectively, and the power densities are 36.1, 86.3, 103.8, 165.3 mW/cm^3, respectively. The dependence of energy and power densities on cell-voltage from 0.8 to 1.5 V for FSPSCs is shown in Figure S7. To demonstrate the practical application for energy storage, two FSPSCs were connected in series to power green light-emitting diodes (LED, working voltage: 1.5 V) as shown in Figure 4h. Here we found that this device could power a green light-emitting diode (LED) for 10 min after charging at 4 mA/cm^2 for 1 min.

The long-term cycling stability of the FSPSC was evaluated by CV tests at a high scan rate of 100 mV s^{-1}. As shown in Figure 4*i*, no matter what the test condition is, the C_{sp} of this FSPSC device almost retains about 100% of the initial value after 1500 cycles at the normal state. Then, the FSPSC device was continuously tested for 1500 cycles under the bent state and 1500 cycles under the fold state. Finally, the FSPSC recover to the normal state to have final 1500 cycles. Only 3.6% of the initial

C_{sp} was lost after the above 6000 cycles as shown in Figure 4*i*, and the surface morphology of MnO_2 layers is still kept well and almost unchanged as shown in SEM in Figure S8. This result shows the assembled FSPSC has an excellent long-term cycle performance and confirms its potential application in the flexible energy storage.

In summary, the novel multi-layered MnO_2/Ni/graphite/paper electrodes were fabricated by sequentially coating graphite layer, Ni layer, and MnO_2 layer on the ordinary cellulose paper. The composite electrodes show light, thin, low cost, flexible and high electrochemical performance. The solid-state FSPSCs based on the MnO_2/Ni/graphite/paper electrodes were assembled, and they showed large volumetric C_{sp} (1020 mF/cm^3 at 5 mV/s), large energy and power densities (energy density of 106 mWh/cm^3 (66.2 Wh/kg) and power density of 48 mW/cm^3 (60.0 kW/kg) and superior long-term cycle stability (less 4% loss of the maximum C_{sp} after 6000 cycles). These findings indicate the designed MnO_2/Ni/graphite paper electrodes are promising materials for FSPSCs. The reported design concept of electrode also can be utilized to other metal oxides, such as Co_3O_4, NiO, and V_2O_5, to build the hybrid paper electrode, which will be promising for a large number of device applications, such as batteries and sensors.

Experimental Section

Fabrication of the multi-layered MnO_2/Ni/graphite/paper electrodes: All reagents utilized in this study were analytical grade and were used directly without any purification. The normal cellulose papers (A4 print papers) were purchased from the supermarket of South China Normal University in Guangzhou in China. The homogeneous graphite layer on paper was firstly fabricated by following procedures: the cellulose paper was drawn again and again by the graphite rod to get the graphite stripes. Each stripe was guided by a plastic ruler and repeat for 5 times. The stripes all were closed to each others. After drawing, the paper was cleaned by dipping 1 min in distilled water, ethanol, and acetone, respectively, and then rinsed in distilled water for 1 min. Then the homogeneous Ni layer was fabricated on graphite/paper by galvanostatic electrodeposition in a conventional three-electrode glass cell at 70 ^{0}C for 32 min. The anode is a Ni foil (99.9%, 1.8 cm^2), and the saturated calomel electrode (SCE) was

used as reference electrode that was connected to the cell with a double salt bridge system. The current density for electrodeposition is 20 mA/cm^2. The deposition solution is 0.8 M $NiSO_4 \cdot 6H_2O$+0.35 M $NiCl_2 \cdot 6H_2O$+0.65 M H_3BO_3+3.47×10^{-5} M sodium dodecyl sulfate (pH=3~4) at 25°C. Electrodeposition of MnO_2 layer was performed on the Ni/graphite paper to fabricate the sandwich-structured MnO_2/Ni/graphite paper at a current density of 1.0 mA/cm^2 in solution of 0.01 M $MnAc_2$+0.02 M NH_4Ac+dimethyl sulfoxide (10%) at 70 ^{0}C for 30 min. A graphite rod (spectrum grade, Shanghai, China) of 4.0 cm^2 was used as counter electrode in this experiment.

Characterization: The surface morphologies and microstructures of the multi-layered MnO_2/ Ni/graphite/paper electrodes were characterized by field emission scanning electron microscopy (FE-SEM, JSM-6330F) and X-ray diffraction (XRD, D8 ADVANCE). The chemical state and compositions of products were analyzed using Raman Spectroscopy (Renishaw inVia) and X-ray Photoelectron Spectroscopy (XPS, ESCA Lab250). The surface area of the product was calculated from nitrogen adsorption/desorption isotherms at 77 K that were conducted on an ASAP 2020 V3.03 H instrument. Prior to measurement, all samples (powders) were outgassed at 100 ^{o}C for 300 min under flowing nitrogen. Inductively coupled plasma atomic emission spectroscopy (ICP, SPECTRO) was used to analyze the actual loading of Ni and MnO_2 on the conductive substrates. The mass of graphite was measured by using the electronic balance (ESJ210-4, Shenyang China).

Fabricating solid electrolyte and assembling the SCs: The solid-state flexible symmetrical planar SC devices were assembled by separating two paper electrodes with a filter paper (Shuangquan Brand, China Hangzhou). The area ratio of negative electrode to positive electrode was fixed to be 1:1, in order to balance the charge between the electrodes. Carboxymethyl cellulose sodium (CMC)/Na_2SO_4 gel was utilized as solid-state electrolytes for SC devices. The CMC/Na_2SO_4 gel was prepared by mixing CMC (3 g) and Na_2SO_4 (3 g) in deionized water (50 mL) and heated at 85 °C for 3 h under vigorous stirring. Prior to the assembling, the electrodes and separator were soaked with the CMC/ Na_2SO_4 solution and then allowed to solidify at room temperature for 6 h. Finally, the planar SCs were

assembled and then were heated at 45 °C for 12 h to remove excess water in the electrolyte.

Electrochemical measurements: Electrochemical performance of the MnO_2/Ni/graphite/paper electrodes was studied with a CHI760D electrochemical workstation (Chenhua, Shanghai) by cyclic voltammetry and charge-discharge measurements in a conventional three-electrode cell. The three-electrode cell consisted of Pt as the counter electrode, the saturated calomel electrode (SCE) as the reference electrode and the multi-layered MnO_2/Ni/graphite/paper electrodes as the working electrodes. A solution of 0.5 M Na_2SO_4 served as the electrolyte at 25 °C. The electrochemical performance of the assembled FSPSCs device was investigated via cyclic voltammetry and charge-discharge measurements in a two-electrode system. Cyclic voltammograms (CVs) were recorded between 0 and 0.8 V at scan rate of 5 to 100 mV/s. Galvanostatic charge-discharge testing of MnO_2/Ni/graphite/paper electrodes was conducted between 0 and 0.8 V *vs* SCE at current density of 0.5~4.0 mA/cm^2 and that of FSPSCs device was conducted between 0 and 1.2 V *vs* SCE at current density of 0.5~4.0 mA/cm^2. The cycling performance was tested by cyclic voltammetry sweeps at a scan rate of 100 mV/s for 6000 cycles.

Acknowledgements

This work was supported by NSFC (51173212 and 21073240), Natural Science Foundation of Guangdong Province (S2013020012833), Fundamental Research Fund for the Central Universities (13lgpy51), Fund of New Star Scientist of Pearl River Science and Technology of Guangzhou (2011J2200057), SRF for ROCS, SEM ([2012]1707), and Open-End Fund of State Key Lab of Physical Chemistry of Solid Surfaces of Xiamen University (201113).

References

1 Qin, X. D. Wang and Z. L. Wang, *Nature.,* 2008, **451**, 809-813.

2 K. Wang, Q. Meng, Y. Zhang, Z. Wei, M. Miao, *Adv. Mater.,* 2013, **25**, 1494-1498.

3 Y. L. Yuan, B. Yao, B. Hu, K. F. Huo, W. Chen, J. Zhou, *Energy Environ. Sci.,* 2013, **6**, 470-476.

4 Y. Li, Z. Li, P. K. Shen, *Adv. Mater.,* 2013, **25**, 2474-2480.

5 F. Liu, S. Song, D. Xue, H. Zhang, *Adv. Mater.,* 2012, **24**, 1089-1094.

6 Z. Weng, F. Li, D.-W. Wang, L. Wen, H.-M. Cheng, *Angew. Chem. Int. Edit.,* 2013, **52**, 3722-3725.

7 Q. Lu, J. G. Chen, J. Q. Xiao, *Angew. Chem. Int. Edit.,* 2013, **52**, 1882-1889.

8 M. Gimenez-Lopez, A. L. Torre, M. W. Fay, P. D. Brown, A. N. Khlobystov, *Angew. Chem. Int. Edit.,* 2013, **52**, 2051-2054.

9 Y. Cheng, S. Lu, H. Zhang, C. V. Varanasi, J. Liu, *Nano Lett.,* 2012, **12**, 4206-4211.

10 H. Ji, L. Zhang, M. T. Pettes, H. Li, S. Chen, L. Shi, R. Piner, R. S. Ruoff, *Nano Lett.,* 2012, **12**, 2446-2451.

11 R. B. Rakhi, W. Chen, D. Cha, H. N. Alshareef, *Nano Lett.,* 2012, **12**, 2559-2567.

12 J. Jiang, Y. Li, J. Liu, X. Huang, C. Yuan, X. Wen. Lou, *Adv. Mater.,* 2012, **24**, 5166-5180.

13 L. Nyholm, G. Nyström, A. Mihranyan, M. Strømme, *Adv. Mater.,* 2011, **23**, 3751-3769.

14 L. Yuan, X. Xiao, T. Ding, J. Zhong, X. Zhang, Y. Shen, B. Hu, Y. Huang, J. Zhou, Z. L. Wang, *Angew. Chem. Int. Edit.,* 2012, **51**, 4934-4938.

15 L. Peng, X. Peng, B. Liu, C. Wu, Y. Xie, G. Yu, *Nano Lett.,* 2013, **13**, 2151-2157.

16 J. J. Yoo, K. Balakrishnan, J. Huang, V. Meunier, B. G. Sumpter, A. Srivastava, M. Conway, A. L. M. Reddy, J. Yu, R. Vajtai, P. M. Ajayan, *Nano Lett.,* 2011, **11**, 423-1427.

17 C. Meng, C. Liu, L. Chen, C. Hu, S. Fan, *Nano Lett.,* 2010, **10** , 4025-4031.

18 H. Gwon, H. Kim, K. U. Lee, D.-H. Seo, Y. C. Park, Y.-S. Lee, B. T. Ahn, K. Kang, *Energy Environ. Sci.,* 2011, **4**, 1277-1283.

19 L. Yuan, B. Yao, B. Hu, K. Huo, W. Chen, J. Zhou, *Energy Environ. Sci.,* 2013, **6**, 470-476.

20 H. Dai, *Acc. Chem. Res.*, 2002, **35**, 1035-1044.

21 G. Zheng, L. Hu, H. Wu, X. Xie, Y. Cui, *Energy Environ. Sci.,* 2011, **4**, 3368-3373.

22 Z. Yu, B. Duong, D. Abbitt, J. Thomas, *Adv. Mater.,* 2013, **25**, DOI: 10.1002/adma.201300572.

23 L. B. Hu, J. W. Choi, Y. Yang, S. Jeong, F. La Mantia, L. F. Cuiand, Y. Cui, *Proc. Natl. Acad. Sci. U. S. A.,* 2009, **106**, 21490–21494.

24 X. Lu, T. Zhai, X. Zhang, Y. Shen, L. Yuan, B. Hu, L. Gong, J. Chen, Y. Gao, J. Zhou, Y. Tong, Z. L. Wang, *Adv. Mater.,* 2012, **24**, 938-944.

25 J. Liu, J. Jiang, C. Cheng, H. Li, J. Zhang, H. Gong, H. J. Fan, *Adv. Mater.,* 2011, **23**, 2076-2081.

26 G. Yu, L. Hu, N. Liu, H. Wang, M. Vosgueritchian, Y. Yang, Y. Cui, Z. Bao, *Nano Lett.,* 2011, **11**, 4438-4442.

27 G. Yu, L. Hu, M. Vosgueritchian, H. Wang, X. Xie, J. McDonough, X. Cui, Y. Cui, Z. Bao, *Nano Lett.,* 2011, **11**, 2905-2911.

28 J.-H. Kim, K. H. Lee, L. J. Overzet, G. S. Lee, *Nano Lett.,* 2011, **11**, 2611-2617.

29 L. Bao, J. Zang, X. Li, *Nano Lett.,* 2011, **11**, 1215-1220.

30 Y. Hou, Y. Cheng, T. Hobson, J. Liu, *Nano Lett.,* 2010, **10**, 2727-2733.

31 X. Lu, X. Huang, S. Xie, T. Zhai, C. Wang, P. Zhang, M. Yu, W. Li, C. Liang, Y. Tong. *J. Mater. Chem.,* 2012, **22**, 13357-13364.

32 (a) M. Toupin, T. Brousse , D. Belanger. *Chem .Mater*., 2004, **16**, 3184-3190. (b) J. K. Chang, M. T. Lee, W. T. Tsai, M. J. Deng, L. W. Sun. *Chem. Mater.*, 2009, **21**: 2688-2695.

33 M. H. Yu, T. Zhai, X. H. Lu, X. J. Chen, S. L. Xie, W. Li, C. L. Liang, W. X. Zhao, L. P. Zhang, Y. X. Tong. *J. Power Sources.*, 2013, **239**, 64-71.

34 H. Zhu, X. Wang, X. Liu, X. Yang, *Adv Mater*. 2012, **24**, 6524-6529.

35 J. X. Zhu, W. H. Shi, N. Xiao, X. H. Rui, H. T. Tu, X. H. Lu, H. H. Hu, J. Ma, Q. Y. Yan, *ACS. Appl. Mater. Interfaces.,* 2012, **4**, 2769-2774.

36 W. Chen, R. B. Rakhi, H. N. Alshareef, *J. Mater. Chem*., 2012, **22**, 14394-14402.

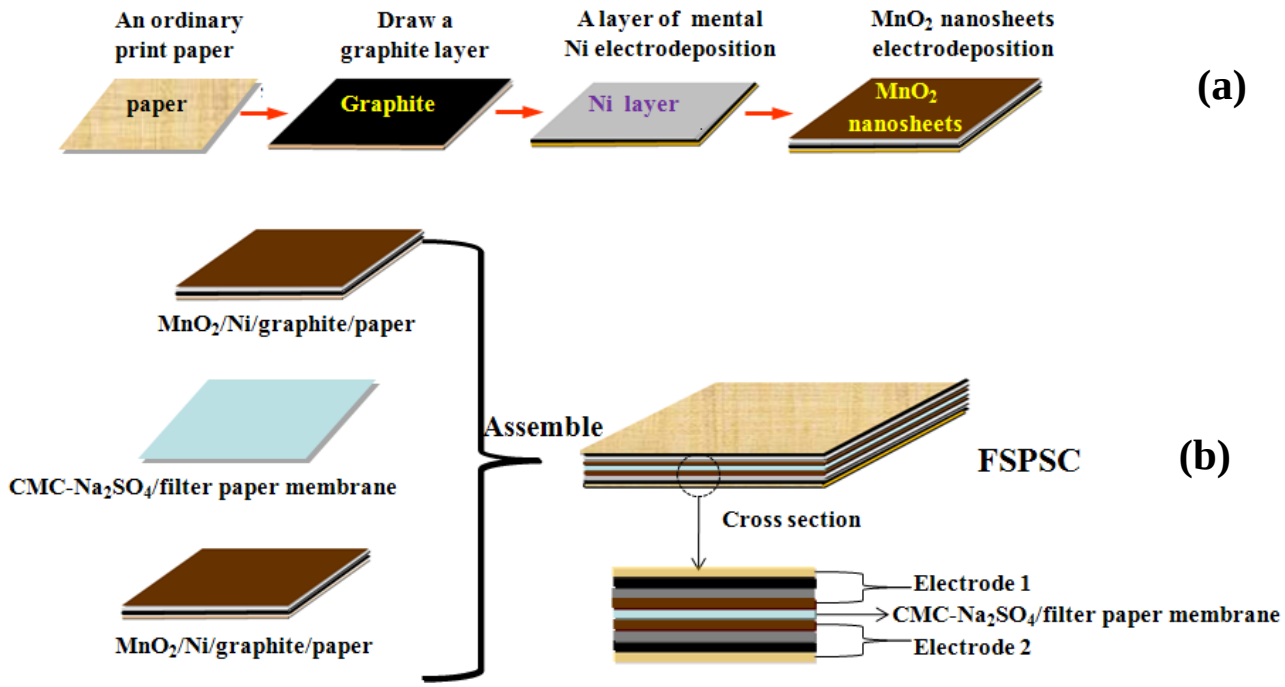

Scheme 1. (a) The procedures utilized to fabricate the sandwich-structured MnO_2/Ni/graphite/paper electrode; (b) the assemble of flexible symmetrical planar supercapacitor (FSPSC).

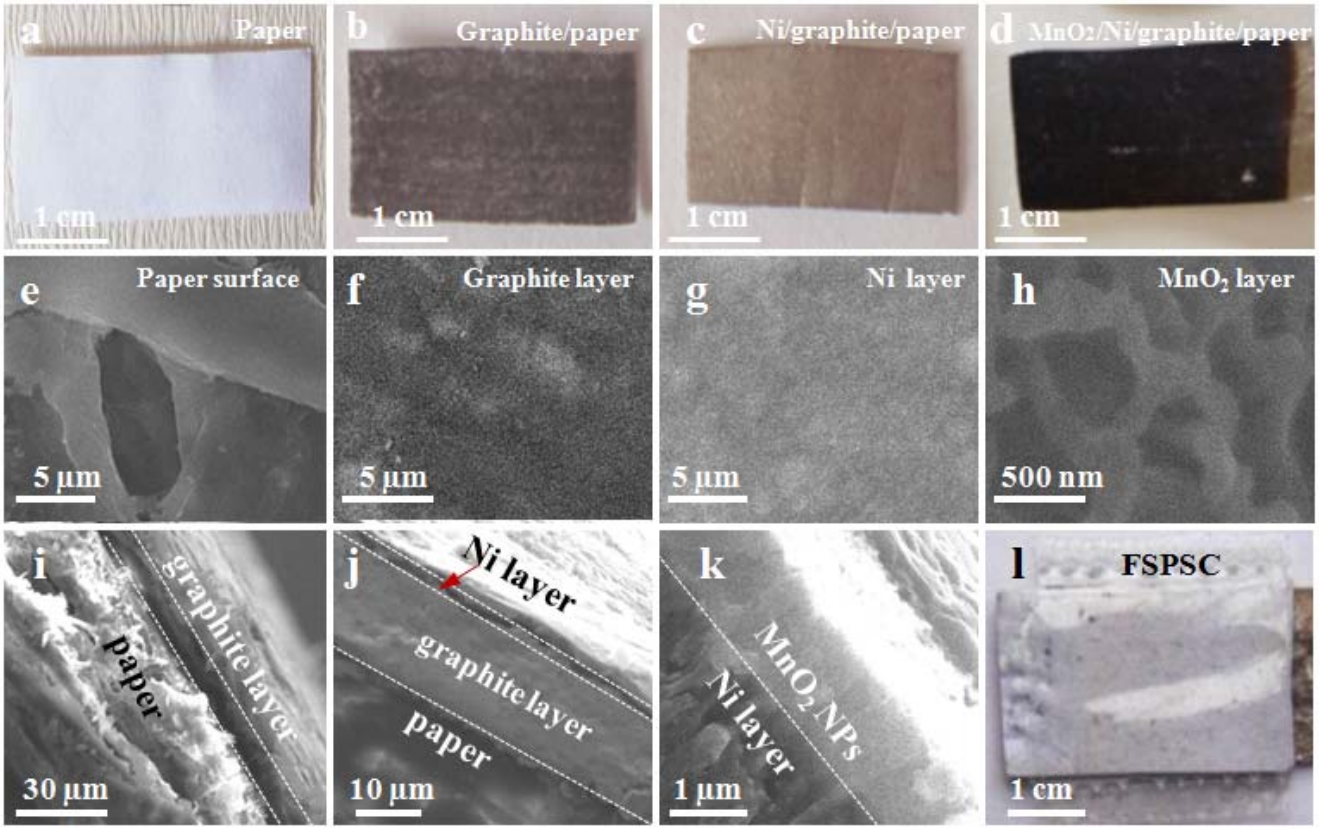

Figure 1. Optical image of (a) paper, (b) graphite/paper, (c) Ni/graphite/ paper and (d) MnO_2/Ni/graphite/paper; SEM images of (e) paper, (f) graphite/paper, (g) Ni/graphite/paper and (h) MnO_2/Ni/graphite/paper surface; SEM images of (i) cross section of the graphite/paper, (j) cross section of the Ni/ graphite/paper and (k) interfacial part between Ni and MnO_2 layers; (l) Optical image of the flexible symmetrical planar supercapacitor (FSPSC).

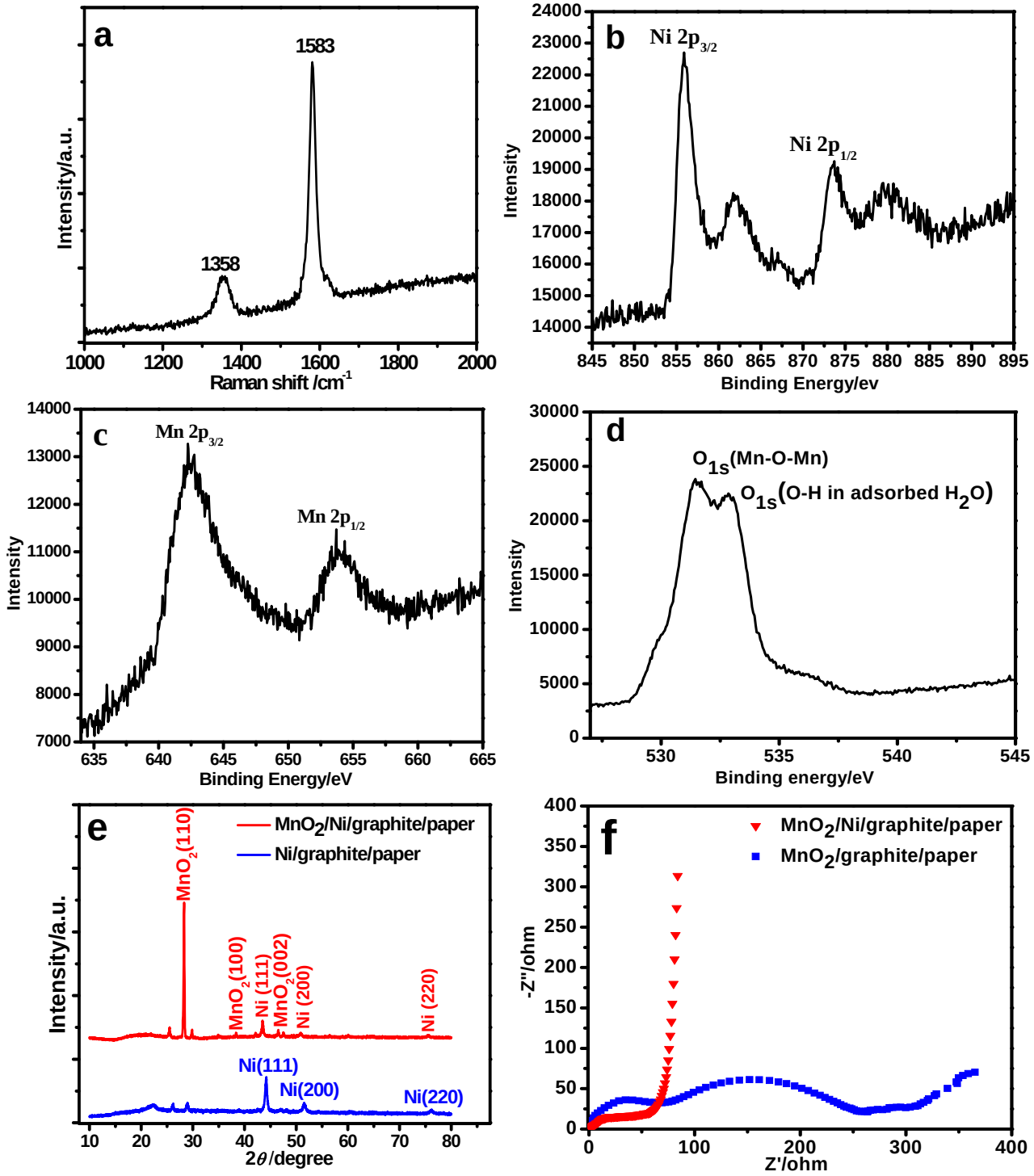

Figure 2. (a) Raman spectrum of the graphite layer; (b-d) XPS spectra of Ni 2p, Mn 2p, and O 1s of electrode; (e) XRD spectra of the paper electrodes before and after electrodeposition of MnO_2 layer; (f) ESI curves of the paper electrodes with and without Ni layer.

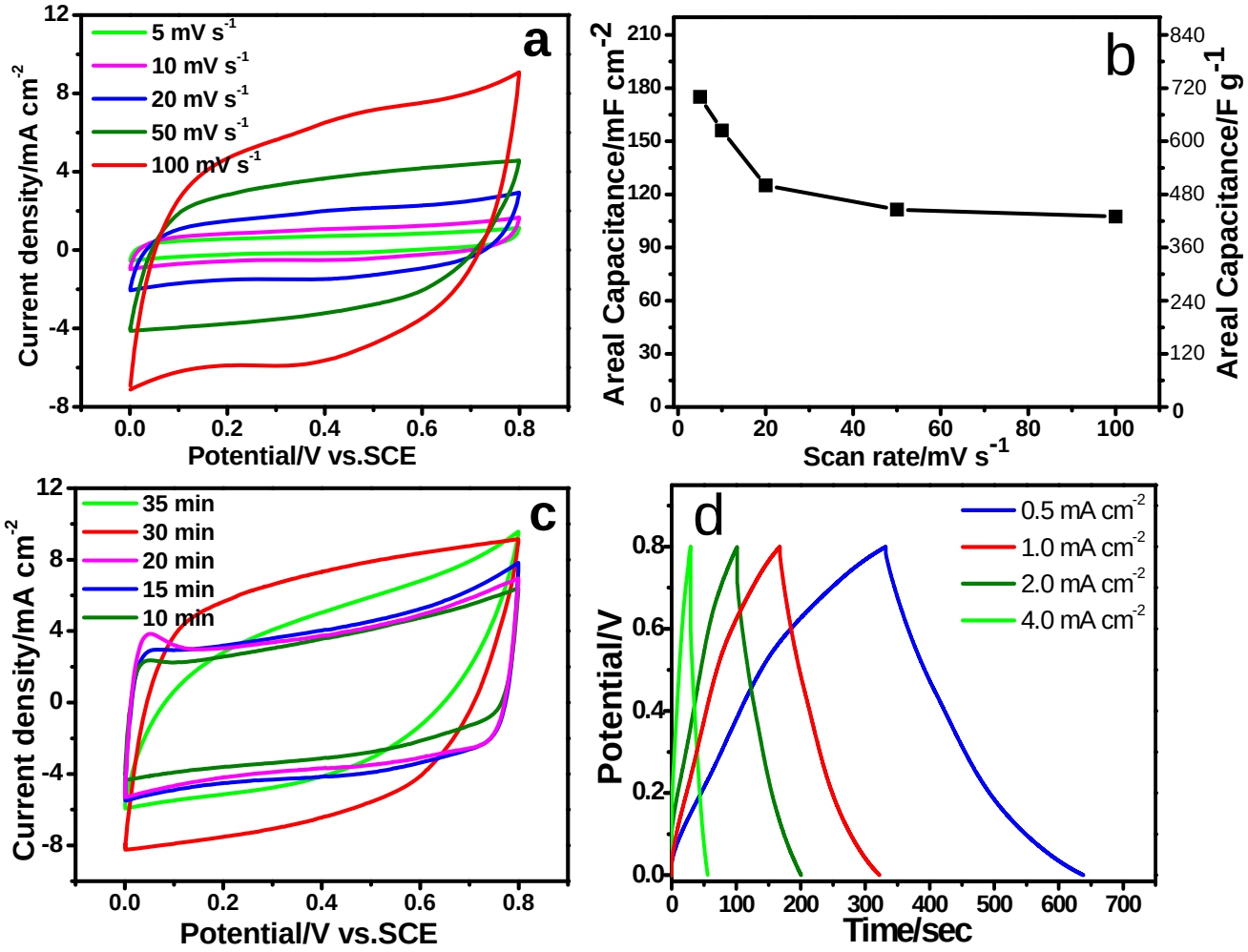

Figure 3. (a) CVs of the MnO_2/Ni/graphite/paper electrode at different scan rates; (b) Plotted curve of the variation in C_{sp} of the paper electrode as a function of scan rate; (c) CVs of the paper electrode with different electrodeposition time of MnO_2 in 0.5 M Na_2SO_4 aqueous solution at 100 mV/s; (d) Galvanostatic charge-discharge curves of the paper electrode at different current densities.

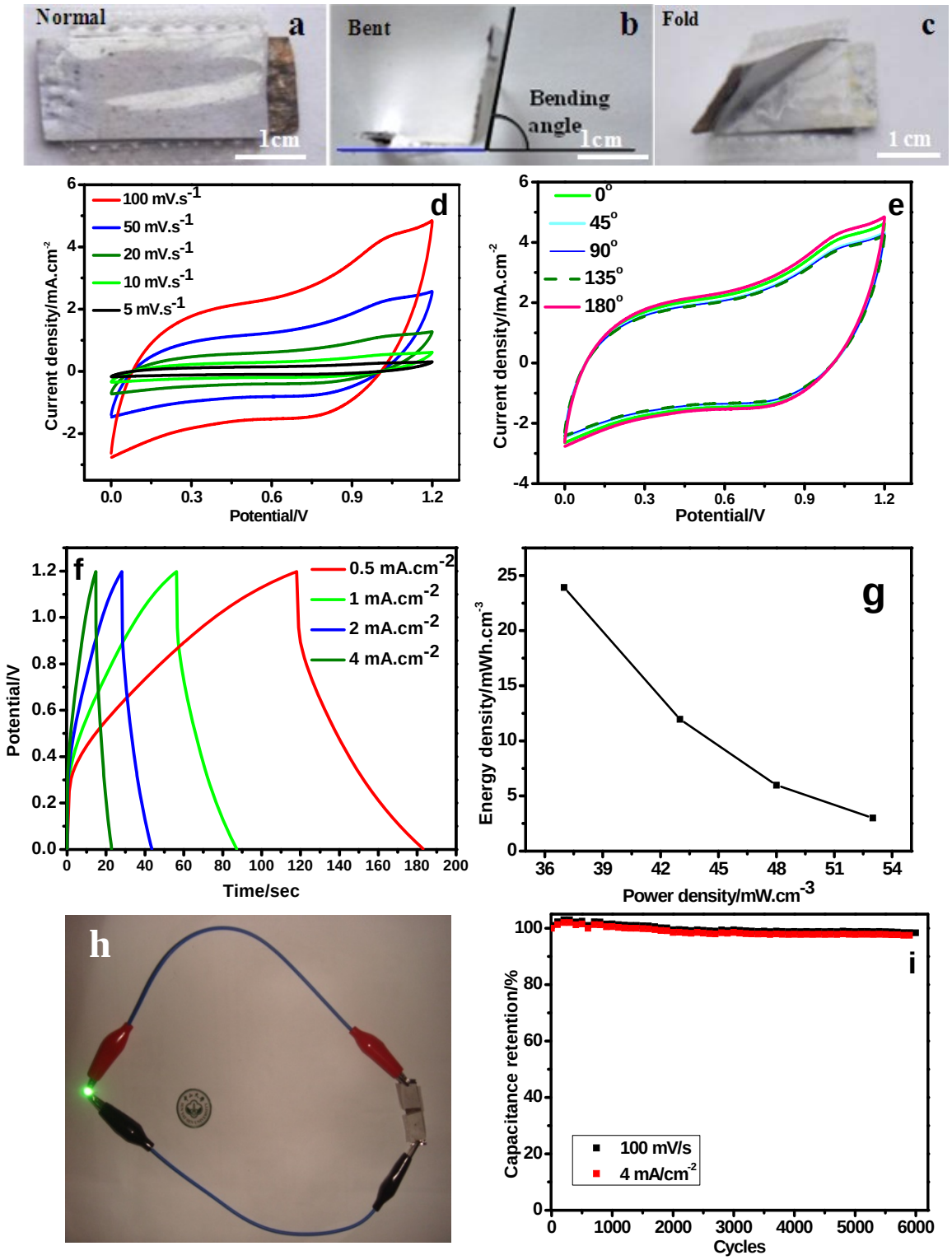

Figure 4. Situations of the FSPSC (a) Normal; (b) bent; (c) fold; (d) CVs of the FSPSC in CMC-Na_2SO_4 solid-state electrolyte and different scan rates; (e) CVs of the SPESC at different situations (bent, twist and fold); (f) Galvano-static charge-discharge curves of the FSPSC under different current density; (g) C_{sp} of the SPESC as a function of scan rate; (*h*) Summary plots of C_{sp} at different current densities for the FSPSC. Light-emitting diode (LED) lighting demonstration, with the diode driven by 2 FSPSCs in series (insert); (*i*) Cycling performance of the FSPSC for 3000 cycles at 100 mV/s.

TOC GRAPHICS

We develop a cheap and simple drawing-electrodeposition method to fabricate highly flexible MnO_2/Ni/graphite/paper electrodes and assemble a paper-based energy storage device with specific capacitance and excellent cycle stability.

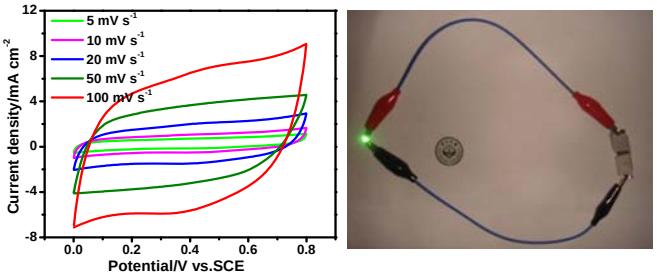

TOC GRAPHICS

We develop a cheap and simple drawing-electrodeposition method to fabricate highly flexible MnO_2/Ni/graphite/paper electrodes and assemble a paper-based energy storage device with specific capacitance and excellent cycle stability.